MXene-based pressure sensor with ultrahigh sensitivity in a small pressure range for voiceless speaking and abnormal writing recognition

Yuzhang Du (yuzhangdu566@nwpu.edu.cn)
Northwestern Polytechnical University
Wenxuan Lu
Northwestern Polytechnical University
Yichen Liu
Northwestern Polytechnical University
Rui Yu
Northwestern Polytechnical University
Panzhen Wu
Northwestern Polytechnical University
Jie Kong
Northwestern Polytechnical University

Research Article

Keywords: MXene, pressure sensors, voice recognition, writing recognition, voiceless, dysgraphia

Posted Date: October 28th, 2023

DOI: https://doi.org/10.21203/rs.3.rs-3470199/v1

Additional Declarations: No competing interests reported.

Version of Record: A version of this preprint was published at Advanced Composites and Hybrid Materials on January 29th, 2024. See the published version at https://doi.org/10.1007/s42114-024-00838-1.

Abstract

Language and characters contain rich information and play an important role in daily communication. Although flexible pressure sensors have aroused extensive attention in information interaction, the application in the special groups who characterized with “voiceless” and/or “dysgraphia” cannot normally speak and/or write is usually ignored. Herein, a high-performance flexible pressure sensor was proposed to learn the expression content from special groups through recognizing the voiceless speaking and abnormal writing. Thanks for the enhanced interfacial interactions and air gaps constructed in device, the as-prepared sensor possesses ultrahigh sensitivity in a small pressure range (S = 45.95 kPa^{-1}, P < 1 kPa) and exhibits an outstanding sensitivity to the slight pressure resulted from voice and writing. In addition, high stability, good flexibility, short response time of 123 ms, and excellent durability over 2000 cycles are also achieved. As the voice and writing detector, it can accurately recognize different voice signals and characters stroke order. Importantly, by comparing with the electrical signals obtained under normal speaking and writing conditions, the real expression content from the special groups can be well acquired. This high-performance pressure sensor, along with its unique structure designing, is expected to be widely used in human − computer interaction, health monitoring, and soft robotics.

1. Introduction

At its broadest definition, “voiceless” is term used to describe those individuals who cannot speak normally owning to some diseases, such as neurodegenerative diseases and the weakness of lip/tongue/palate muscles [1, 2]. “Dysgraphia” is a specific learning disorder in written expression at any stage caused by lack of education and/or diseases, e.g., brain injury, neurologic disease, or degenerative conditions [3, 4]. The emergence of language and characters is not only the symbol of human civilization, but also promotes the exchange of culture and ideas. Although language and characters contain rich information to play an important medium for people to communicate daily, for some special groups characteristic with “voiceless” and “dysgraphia”, they have difficulty to express their intentions through speaking and writing normally [5–7]. In daily life especially in emergency situations, how can others know what the special individual wants to say? Thus, exploiting devices that can translate the physical signals from voiceless speaking and abnormal writing into visualized signals for facilitating communication is urgent and valuable to these special people. Due to the excellent capability of voice and writing recognition, wearable pressure sensors have fixed these problems quite well by translating the external signals and providing meaningful information to the users, guardian, or therapists [8–10]. However, most of the traditional research on pressure sensors focuses solely on foundational sensing tests for common population, ignoring its other applications in the special users.

To minimize the influence of unexpected environmental noises, wearable pressure sensors used for human voice recognition have been usually designed to detect physiological mechanoacoustic signals directly based on the vibrations of vocal cords [11, 12]. As is well known, vibrations of vocal cords and writing are subtle physical signals, namely, the pressure loaded on sensor is very small (P generally less than 1 kPa) [13–16]. There are several capabilities demands for a wearable pressure sensor applied in

voice and writing accurate recognition. Among these key properties, high sensitivity in low pressure range (P within 1 kPa) is the prerequisite for voice and writing perception with a high accuracy level. In recent years, the preparation of high-performance piezoresistive sensors that are characterized by high sensitivity, fast signal response, and stable sensing performance has become a hot topic due to its simple principle [17, 18]. In addition, a simple composition of sensing layer, substrate, and electrodes makes an easy manufacturing process. The sensitivity (S) for piezoresistive sensors is defined as $S=[(R-R_0)/R_0]/\Delta P$ and presents the ability of sensors to convert pressure into electrical signals [19]. Here, R_0 is the electrical resistance without applied pressure, and R presents the electrical resistance of the sensor loaded with a fixed pressure (P), ΔP is the pressure variation. Based on the definition, high sensitivity can be achieved by significantly improving R under a small pressure. However, the use of small pressure to obtain large resistance is often a contradiction. According to the sensing mechanism, the higher R is generally resulted from the effective destruction of conductive paths in sensitive layer, which can be realized under the larger structure deformation caused by a bigger pressure [20, 21]. Therefore, the design of piezoresistive sensors with high sensitivity within small pressure range remains a challenge. Under the external force, enhancing interfacial interactions between conductive substances and polymer substrate is a potential approach to destruct the conductive paths and then to improve resistance change and sensitivity, which is well proven by our works and other researchers [22–25]. Nacre, a regular three-dimensional hierarchical structure consists of ceramic aragonite inorganic materials and biopolymers, is an excellent example of strong interfacial interactions architecture [26]. In this architecture, the soft organic biopolymers act as a medium, allowing for the sliding between ceramic aragonite under the action of external forces [27]. Therefore, enhancing interfacial interactions by simulating nacre-mimetic structure is expected to fabricate ultrahighly sensitive pressure sensors within small pressure range attributed to resistance significant change in sensing layers.

In addition to construct strong interfacial interactions in sensitive layers, microstructure design is another strategy to achieve high sensitivity in pressure sensor.

Among these microstructures, microcone arrays is a classical strategy used for high performance pressure sensor, the top and bottom electrodes with microcone microstructures are pressed together to increase the contact area, which results in electrical resistance decrease and sensitivity improvement [28, 29]. However, mold requirements, photolithography and etching process greatly increase fabrication costs to obtain microcone arrays [30]. Besides, the air gaps between two electrodes need to be very small so that the microcone arrays can be fully contacted under small pressure, the preparation of sensor with small air gaps requires sophisticated fabrication techniques, which hinders the practical applications. Therefore, a simple and cost-effective approach to fabricate the sensors with high sensitivity is essential to meet the requirements of valuable applications. As discussion above, the significant change of electrical resistance in sensitive layers is desired to achieve high sensitivity, but the space allowing for sensitive layers deformation is the prerequisite for electrical resistance significant change under small pressure. Fortunately, the existence of air gaps in device brings enlightenment to prepare highly sensitive pressure sensors by providing enough space for sensing layers large deformation. Consequently, combining the

enhanced interfacial interactions in sensitive layers and the constructed air gaps in device may be an excellent strategy to fabricate pressure sensor with high sensitivity within small pressure region.

In this work, we propose MXene-based flexible piezoresistive sensor with high sensitivity within small pressure region for learning the expression content from the special groups through recognizing voiceless speaking and abnormal writing. Inspired by the intrinsic strong interfacial interactions of nacre's hierarchical structure, the enhanced interfacial interactions in sensing layers were constructed via the formation of hydrogen bonds between MXene nanosheets and PAM polymer. Besides, air gaps were designed between sensing layers and substrate to provide the deformation spacing of sensing layers under small pressure. In this structure, the synergistic effects including of the enhanced interfacial interactions and air gaps endow excellent performances to the sensor. As a result, the ultrahigh sensitivity of 45.95 kPa^{-1} within $P < 1$ kPa, short response and recovery time (123 and 182 ms), good stability, high flexibility, and long-term durability with over 2000 loading/unloading cycles are achieved. In practical application, the extraordinary performances enable the pressure sensor to accurately sense the voice amount, voice frequency, emotion change, environment noise, stroke order of Chinese characters and English words, character size, writing speed, and grip of the pen. By comparing with the electrical signals obtained at normal speaking and writing conditions, the expression content from the special groups with "voiceless" and "dysgraphia" diseases can be learned. So, based on this reported pressure sensor, key information can be translated to others who could timely provide help to these special people especially in time of crisis. In addition, the sensor shows good potential applications in human – computer interaction, health monitoring, and soft robotics.

2. Experimental Section

2.1 Materials

Ti_3AlC_2 powder (particle size 400 mesh, 98%) was gotten from Laizhou Kaiene ceramic Material Co., Ltd. (Jining, China). Acrylamide (99%) was provided by Sigma-Aldrich. Ammonium persulfate (98%), tetramethylethylenediamine (TEMED, 98%), lithium fluoride (LiF, 98%) and concentrated hydrochloric acid were both purchased from Macklin (Shanghai, China). All other reagents were commercial chemicals and utilized as received unless otherwise indicated.

2.2 Preparation of Delaminated $Ti_3C_2T_x$ MXene

Multilayered $Ti_3C_2T_x$ MXene was prepared by selective etching of Al element from Ti_3AlC_2 phase powder via LiF/HCl solution according to the previously reported method [25]. LiF (3.6 g) was dissolved in 40 mL of HCl (9 M), then Ti_3AlC_2 powder (2 g) was slowly added into the above solution and heated at 35°C under stirring for 24 h. After that, the solid residue was centrifuged (3500 rpm, 5 min) and washed with deionized water (DI) until the pH of the suspension reached value of between 4 and 6. The multilayered MXene nanosheets were obtained by drying the solid residue at room temperature. Delaminated MXene was prepared by sonicating the multilayered $Ti_3C_2T_x$ MXene (0.5 g) in DI water (100 mL) for 1 h under an

Ar atmosphere and followed by centrifugation (3500 rpm, 1 h), and the dark green supernatant was collected. Filtering and drying the supernatant at room temperature were applied to obtain the finally delaminated $Ti_3C_2T_x$ MXene that was used for following characterization.

2.3 Preparation of Pressure Sensor

In this work, the pressure sensor with air gaps was fabricated through LBL assembly method by using $Ti_3C_2T_x$ MXene and acrylamide as raw materials. Aqueous solution of acrylamide (100 mg/mL) with ammonium persulfate as initiator and TEMED as catalyst was prepared under ice bath condition. The mixed aqueous solution of MXene was obtained by adding MXene nanosheets (m/m, 10:1) into the above-prepared acrylamide solution. Ploy(acrylamide) (PAM) flexible substrate was firstly prepared by spinning coating acrylamide aqueous solution and then polymerizing acrylamide at 40°C for 60 min (step). Following, 2 mL/per point of acrylamide aqueous solution was slowly added on PAM flexible substrate surface at different sites, pre-polymerization and pre-crosslinking of acrylamide were taken at 40°C for 30 min (step). After that, the mixed solution MXene was coated and then dried at 40°C for 30 min to form the MXene-based sensing layer (step). Finally, the steps and were repeated for three cycles and the whole system was further dried at 40°C for 1h to prepare pressure sensor.

2.2 Characterization

Scanning electron microscope (SEM, FEI Verios G4) was used to observe the morphologies of delaminated $Ti_3C_2T_x$ MXene nanosheets, the structure of the MXene-based sensing layer and the resultant pressure sensor. X-ray photoelectron spectroscopy (XPS), high resolution XPS analyses of the MXene nanosheets and MXene-based sensing layer were investigated on a PHI5400 device (PE Corp., England). X-ray diffraction (XRD) using an X'Pert Pro-diffractometer with Co Kα radiation (λ = 1.5418 Å) was applied to characterize the chemical structure of sensing layer. Thermogravimetric analysis (TGA) (PerkinElmer) was conducted to determine the real mass content of MXene in the sensing layer. The pressure sensor was cut into dumbbell-shaped (20 mm × 2 mm × 0.2 mm, length × width × thickness) for the evaluation of mechanical properties, and all tensile experiments were performed on a universal testing machine (Instron, 2710-004) with a tensile rate of 10 mm/min.

2.3 The Recognition of Voice and Writing

The sensing performance of the sensor was studied by a custom-built cyclic pressure system with controlled force and frequency. The real-time output electric signal was recorded by using high-precision electric signal detection source meter (Keithley, model 2450 and 6514) under the driving voltage of 0.5 V. For voice recognition, the subject was asked to speak some words and sentences in “voiceless” or normal manner, and the pressure sensor was attached on the vocal cords site to monitoring the vibrations of vocal cords. In the writing recognition, the tester wrote Chinese characters and English words directly on the surface of sensor with correct stroke order, error stroke order, different writing speed, various character size and grip of the pen.

3. Results and Discussion

3.1 Fabrication of Pressure Sensor

In this work, to obtain high sensitivity within small pressure range, the enhanced interfacial interactions in MXene-based sensitive layers, as well as air gaps between sensing layers and flexible substrate were constructed in sensor. Nacre, a gold standard for strong interfacial interactions attributed to the bonding effects between aragonite platelets (95 vol%) and nanofibrillar polymer (chitin and proteins, 5 vol%) [31, 32], provides an excellent example and guideline for assembling nanosheets into nanocomposites with high-performance (Fig. 1a). In this architecture, the soft organic biopolymers act as a medium, allowing for the sliding between ceramic aragonite under the action of external forces [27], which offers a new approach to prepare sensors with high sensitivity by facilitating the relative slippage of the adjacent conductive substates in sensing layer. Figure 1b schematically illustrates the key steps for the preparation of pressure sensor by employing $Ti_3C_2T_x$ MXene nanosheets and acrylamide as raw materials through LBL assembly technology. The detailed characterization of the as-prepared $Ti_3C_2T_x$ MXene nanosheets by SEM, EDS mapping, XPS, and high resolution XPS are presented in Fig. S1. The ploy(acrylamide) (PAM) flexible substrate was firstly prepared via spinning coating acrylamide aqueous solution and polymerizing acrylamide at 40°C for 60 min (Fig. b( )). Next, 2 mL of acrylamide aqueous solution per point was uniformly added at different sites on PAM flexible substrate surface (Fig. b( )), pre-polymerization and pre-crosslinking were following taken at 40°C for 30 min. Then, the mixed solution of MXene and acrylamide was uniformly coated, and the MXene-based sensing layer was formed after drying it at 40°C for 30 min (Fig. b( )). The steps and were repeated for three cycles and the whole system was further dried and crosslinked at 40°C for 1h to obtain pressure sensor (Fig. b( )). As shown in Fig. 1c, d and Fig. S2, the resultant sensor exhibits a well-defined multilayer structure, and air gaps are successfully constructed between PAM substrate and MXene-based sensing layers (white arrows indication). Besides, the adjacent sensing layers are tightly jointed by PAM polymer (Fig. 1e), which guarantees the structural stability of device. Uniaxial elongation was applied to measure the flexibility, the pressure sensor possesses excellent stretchability with the elongation up to 138% (Fig. S3), suggesting a good flexibility.

XRD, XPS, and high resolution XPS were applied to verify the hydrogen bonds interfacial interactions between MXene nanosheets and PAM, all data were collected from the sensing layer. Figure 1f shows XRD pattern in the (002) peak for MXene-based sensing layer and pure MXene. As comparing with pure MXene, the main peak (002) of sensing layer clearly downshifts from ≈ 6.4° to ≈ 5.6°, which indicates the increase of full width at half maximum (fwhm) resulted from the inhomogeneity and the spacing increase between MXene nanosheets [23]. The enlarged interlayer spacing strongly suggests that the PAM polymer could intercalate into the adjacent MXene nanosheets and bonding with them. Figure 1g is the element diffraction spectra of the sensing layer and pure MXene. The intensity of O 1s and C 1s diffraction peaks from sensing layer is obviously stronger by comparing with pure MXene. Due to the percentage of C and O elements in PAM polymer is higher than that of MXene, the formation of PAM polymer increases the proportion of C and O elements and then leads to the decreased percentage of Ti element in sensing layer. TGA analysis was used to evaluate the real mass content of MXene in sensing layer, and MXene mass content of about 92% is consistent with the theoretical mass ratio (Fig. S4). The hydrogen bonding

between PAM and MXene nanosheets was analyzed on high resolution XPS. As shown in Fig. 1h and i, diffraction peak of O element obtained from sensing layer upshifts from 527.1 eV to 529.4 eV (Fig. 1h), at same time, diffraction peak assigned to F element shows a similar increase from 683.2 eV up to 684.6 eV (Fig. 1i). These increases indicate that the electron-loss behavior of O and F atoms caused by H atom attraction effect after the formation of − H···O and − H···F between PAM chains and MXene nanosheets [33]. The above results demonstrate the formation of PAM polymer in sensing layer and bonding with MXene nanosheets via hydrogen bonds. There are reasons to believe that the synergistic effects of enhanced interfacial interactions in sensing layer and air gaps in device will be benefit to improve the sensing performance.

3.2 Ultrahigh Sensitivity and Good Sensing Performance

As discussion above, the high sensitivity in small pressure region is the key character for pressure sensor to realize real-time, accurate, and reliable monitoring of the tiny pressure. So, some quantitatively important parameters including of sensing sensitivity (S), stability, response time, cycle stability, and flexibility are employed to evaluate the comprehensive performances and practicability of the resultant pressure sensor [34]. Figure 2a presents the current versus changed voltage under various pressures (pressure = 0.014, 0.085, 0.284, 1.20, 1.79, 2.00, 3.90, and 4.21 kPa) with the voltage varying from − 5.0 to 5.0 V. The linear dependence of voltage on the current under various external pressures indicates a good ohmic contact between the sensing layer and the electrodes, which is a guarantee for effective evaluation of sensor performance. The curves of $\Delta R/R_0$ as a function of the applied pressures in the range of 0.014 − 7.45 kPa is shown in Fig. 2b. Electrical signals exhibit good repeatability when the sensor is subjected to the small pressures less than 1 kPa (0.014, 0.085, 0.284, 0.893 kPa) and the higher pressures larger than 1 kPa, implying the outstanding response performance. Sensing sensitivity (S), defined as $S=[(R-R_0)/R_0]/\Delta P$, is a key performance parameter describing the ability of the pressure sensor to convert external pressure into electrical signal. For tiny pressure perception, high sensitivity in small pressure rang is the basic to device for realizing perfect sensing performance. In various pressure ranges of 0.014 − 0.089 kPa and 1.20 − 7.45 kPa, $\Delta R/R_0$ showing linear increase with different slopes are clearly observed (Fig. 2c). Within the range of pressure less than 1 kPa, ultrahigh S of 45.95 kPa^{-1} (linear fit, R^2 = 0.9950, Fig. 2c) is higher than that of the previously reported tiny pressure perception sensors (e.g., sound recognition sensors, Fig. 2d) [33, 35–45], demonstrating the ultrahigh sensing sensitivity within small pressure range of the resultant pressure sensor. Although $\Delta R/R_0$ also presents linear increase in pressure range of 1.20 − 7.45 kPa (Fig. 2c), the sensor has lower S of 5.03 kPa^{-1} (linear fit, R^2 = 0.9910). Stability and reliability are also important properties for sensors in practical applications. When loading P = 0.893 kPa on the pressure sensor for about 4s, the $\Delta R/R_0$ maintains a constant value until the external force removed (Fig. 2e). The excellent stability and reliability were further approved by the resistance change under changed pressures (Fig. 2f). $\Delta R/R_0$ increases up to 25 and holds this value for about 3s by applying 0.248 kPa on sensor. Following, with increasing pressure to 7.45 kPa, the $\Delta R/R_0$ is improved up to about 90 and keeps this value for 3s, and then the value rapidly decreases to 20 once pressure reduced to 0.085 kPa. In addition, the pressure sensor preforms fast responsiveness to the small pressure (P = 0.893 kPa) with a

short response time of 123 ms and recovery time of 182 ms (Fig. 2g). The 2 000 cycles of loading and unloading were conducted to evaluate the service life and durability of the sensor (Fig. 2h). After 2 000 cycles, the output current signal of the sensor remains stable, and the attenuation of the electrical signal is negligible, suggesting the excellent durability under dynamic condition.

3.3 Sensing Mechanism

A possible model of the sensing mechanism based on crack-propagation is proposed in Fig. 3 to illustrate the changes of conductive paths in the sensing layer. In this work, the ultrahigh sensitivity in a small pressure range is achieved benefited from the synergistic effects of the enhanced interfacial interactions in sensitive layer and the air gaps in device. These factors govern the response of conductive paths to the deformation under the applied pressure [22, 25, 46]. According to the definition of sensitivity (S), S can be significantly improved through enlarging the resistivity change with a small pressure loading. Hence, the easily deformation of sensing layer is the foundation to the resistance change especially in the small pressure region. The constructed air gaps (Fig. 3a and b) provide the space to facilitate the deformation of sensing layer along the force direction, which firstly guarantees the destruction of MXene conductive paths. In addition, based on our design strategy for sensing layer, PAM polymer with little mass percentage (about 8%) act as medium was bonded with MXene nanosheets, resulting in sensing layer with a compact rather than a loose structure due to the stronger interfacial interactions (Fig. 3c). Benefiting from the hydrogen bond interfacial interactions approved in Fig. 1f-i, the sliding of the adjacent MXene nanosheets is improved owning to the stretchability and tractive effort of the PAM polymer chains, which causes the partial destruction of conductive paths. With increasing pressure to 0.893 kPa, a relative loose structure of sensing layer can be clearly observed (Fig. 3d and f), suggesting that the more cracks are produced in the entire sensing layer (Fig. 3e). At this moment, due to the largest number of cracks generation, the highest resistance in sensing layer and ultrahigh sensitivity of $S = 45.95\ kPa^{-1}$ of sensor are achieved. After that, if a bigger force further applied on the pressure sensor, few conductive paths could be destructed because that PAM polymer chains will be further stretched to dissipate the external force at this moment, producing a relatively small sensitivity of $5.03\ kPa^{-1}$ when the pressure larger than 1 kPa. In addition, after removing the pressure, the synergistic effects from air gaps and interfacial interactions facilitate the structure recovery of device, which endows good stability and reliability to sensor.

3.4 Voiceless Speaking Recognition

Among the various biosignals, language contains a wealth of content for daily information exchange in time and amplitude domains [47]. However, for some special groups characterized with “voiceless”, they cannot speak normally owning to some neurodegenerative diseases and the weakness of lip/tongue/palate muscles [1]. In view of this situation, real-time and accurately learning their expression content will be very valuable for those special people’s especially in a time of crise. So, because of its ultrahigh sensitivity within small pressure range, the as-prepared pressure sensor used as a voice recognition device was systematically investigated via the monitoring of vocal cords vibrations.

The response of sensor to the Chinese phonetic alphabet and words, as well as English letters and words were firstly tested to evaluate the basic ability of voice recognition. As shown in Fig. S5, different tone “ā, á, ǎ, à” of Chinese phonetic alphabet “ ” induce similar signal peak but produce various $\Delta R/R_0$ values. For different tone, “á” or “à” possesses a relative higher volume and then loads bigger pressure on sensor, so the larger $\Delta R/R_0$ is produce. In addition to Chinese phonetic alphabet, the sensor responses well to English letters, twenty-six letters cause twenty-six different waveforms (Fig. S6). The highly sensitive to voice was also proved by the identification of Chinese and English words (Fig. 4a-e). When the subject said “ , , , ” and “ , , , ”, respectively, single signal peak corresponding to every Chinese word repeats well (Fig. 4a and b), while, the English word produces electrical signal with multiple characteristic peaks. By comparing the electrical signals induced by Chinese words and English words, the obvious difference may be attributed to the following reasons. Chinese words are all mono-syllabic and encompass four pronunciation tones [48], which is different from the English words characterized with the combination of both mono-syllabic and polysyllabic, therefore, each Chinese word can produce its own unique single peak signal. The above results demonstrate the resultant pressure sensor has great potential application in “voiceless” speaking recognition for the special groups. Consequently, the “voiceless” speaking from special group in a state of crisis situations was simulated and recognized. As shown in Fig. 4e and f, there is a good coincidence between the curves of voiceless and normal speaking regardless of the Chinese phrase “ , , , ” and sentences “ ”, “ ”, as well as English sentences “It is a sunny day”, “This is a pressure sensor”. Therefore, by comparing with the normal speaking curves, the real expression content of “voiceless” speaking can be accurately recognized, suggesting that the sensor has great value to the special groups.

Generally, each person's voice has different characteristics. For example, men and women has different tones, and man's voice is more vigorous. Figure 5a and b show the comparison of voice signals from men and women. Signal with sharp peak is obviously observed in the curves from the man’s voice (M, n and M, v) due to the bigger pressure loaded on sensor, indicating that the device has a good ability to distinguish the gender of the speaker. However, regardless of man or woman, there is a high degree of consistency between the voiceless and normal speaking curves, besides, all curves have good agree with the spectrum signals obtained from Adobe Audition. Emotion detection is especially helpful to these special groups, such as voiceless personal, patients suffering from mental diseases, and empty nesters living alone. Changes in mood during speaking can be well emerged via sound volume and/or frequency [49]. To prove the usability for emotion detection based on voice signals, we used the pressure sensor to record voiceless speaking with various sound volume or frequencies. As shown in Fig. 5c and d, sensor has excellent capability to differentiate sound volume and frequencies. With increasing volume and frequency, the value and the number of signal peak are significantly improved, respectively. A wind-rose map was used to display the form of emotion changes resulted from the detection of voiceless speaking with different volume and frequencies, in which the volume and frequency of the sound signal can be represented by the length and width of the petals (Fig. 5e). Based on this visual diagram, relaxed, calm, and nervous emotion can be distinguished easily, providing a basis for whether help and emotion care need to be gave to these special personal. In daily life, the sound from the animals is ubiquitous (e.g., dog, cat, bird, and so on).

Although, natural sound has been proved to help to alleviate the increasing mental health and anxiety problems of modern people, while it is easy to cause interference to the voice recognition and is usually regarded as environment noise.[50] To minimize the influence of unexpected environmental noises, voice recognition sensors should possess the capability to distinguish animal's sounds. The response signals from different animal sounds (dog, cat, bird, and sheep) are shown in Fig. 5f. Superior detecting performance is revealed by the as-prepared pressure sensor through recognizing animal acoustic activities. The signals with multiple characteristic peaks not only exhibit excellent repeatability and good consistency with the spectra recorded from Adobe Audition, but are obviously different from the curves of human voice. That is to say, by taking advantage of the waveform analysis, it is easy to distinguish whether the sound comes from person or environment. Thus, based on these above results, the pressure sensor reported in this work is expected to help the special groups to transmit information or communicate.

3.5 Abnormal Writing Recognition

In addition to language, character is another main form of daily communication. Nevertheless, some people suffer from "dysgraphia", indicating that they have specific disorder in written expression due to diseases and/or lack of adequate education. Consequently, for these special groups, applying pressure sensors to capture the important information that they want to express will be of great help in their lives. For writing, the correct stroke order plays a decisive role to the accurate formation of character especially for Chinese characters. So, high recognition performance of strokes is the prerequisite for writing identification. Figure 6 shows the excellent capability for the recognition of stroke order of different Chinese characters " , , , " and the corresponding English words. The stroke types and order of Chinese character " " is presented in Fig. 6a up. Taking " " as an example, single or multiple characteristic peaks correspond well to the various strokes. It is a basic feature of writing that the amount of force applied is different at the different parts of stroke. For Chinese character stroke, the starting, closing, turning, and hook points are usually powerful, means that the relative bigger pressure will load at these places. As shown in Fig. 6b, the Chinese character stroke " " possesses , , and three power points, and every point induces one characteristic peak. Similar, the English word "mom" consists three letters of "m", "o" and "m", two different waveforms are produced by letters "m" and "o" (Fig. 6c). Moreover, , , and three power points from letter "m" results in three characteristic peaks (Fig. 6d). The as-prepared sensor can accurately recognize Chinese words " , " and the corresponding English letters (Fig. 6e–h). In addition, if write a character with error stroke order (Fig. 6i–k), the sensor shows similarly high recognition capability. For example, the writing of Chinese character " " should to follow the stroke order from 1 to 7 (Fig. 6i up). The waveform induced by the writing with error stroke order significantly differs that produced by the correct writing (Fig. 6i). However, whether writing with correct or error stroke order, the characteristic peak has good agree with the corresponding stroke. All above results demonstrate the pressure sensor has high sensing performance of stroke monitoring and shows a great potential in writing recognition for special groups with dysgraphia.

Poor hand strength and endurance is often the cause of dysgraphia [4, 51]. To simulate the symptom of powerless hand strength and endurance, three different kinds of pen (ballpoint pen, mark pen, and brush pen) were used to write Chinese characters on sensor surface (Fig. 7a). Because of the difference of tip hardness (ballpoint pen mark pen brush pen), the lower hardness will apply small pressure on sensor and then leads to a little $\Delta R/R_0$ value (Fig. 7b). So, in this study, writing with ballpoint pen is regarded as the writing under the normal hand strength. As shown in Fig. 7c, regardless of ballpoint pen, mark pen, or brush pen used to write, all signal curves correspond well to the Chinese character stroke. Besides, the comparison indicates that there is good consistency between signal curves each other no matter whatever kind of pen used. At its broadest definition, dysgraphia is a disorder of writing ability at any stage, the evaluations of character size, writing speed, grip of the pen, and so on, are the expert recommendation for the diagnosis of dysgraphia in clinical application [4]. In this work, writing with too big and too small size, various speed, and the abnormal grip of the pen were simulated to learn the writing content. Figure 8a and b are the signal curves recorded by writing Chinese characters with different size. From these diagrams, the changed size of character can be easily distinguished based on the gaps between the peaks because that a big size needs more time to write at the constant writing speed. Importantly, no matter writing Chinese character with big or small size, there is excellent consistency between these obtained waveforms, which indicates that the writing content can be accurately known by comparing with the electrical signal acquired under the writing with normal size. Similarly, when the pressure sensor used to minor the different writing speed (Fig. 8c), the text content and writing speed are also easily recognized. Figure 8d-f is the response of sensor to the writing with various grip of pen. No matter what way to hold the pen, as long as the subject writes the character completely according to the correct stroke order, all the electrical signals have a good consistency. In a word, by comparing with the signal curve obtained at normal writing condition, the writing content of the special groups with dysgraphia can be accurately read. This perfect performance will provide a great help to these people with disorder of writing ability to express their real intention and emotion.

4. Conclusions

In summary, this work proposes a strategy to learn the real expression content from the special groups with “voiceless” and/or “dysgraphia” diseases by recognizing voiceless speaking and abnormal writing. To achieve this aim, high-performance pressure sensor with ultrahigh sensitivity within small pressure region was designed. Air gaps in device and the enhanced interfacial interactions in sensing layers were constructed to improve the sensing sensitivity. The resultant sensor exhibits ultrahigh sensitivity of 45.95 kPa^{-1} within small pressure range ($P < 1$ kPa), short response and recovery time (123 and 182 ms), good stability, and long-term durability with over 2000 loading/unloading cycles under $P = 0.893$ kPa. For practical application, the sensor possesses excellent performance to sense the simulated “voiceless” speaking and abnormal writing. Due to the highly sensitive to voiceless speaking and abnormal writing, the real expression content from the special people can be accurately acquired.

Declarations

The authors declare no competing financial interests and all data availability without restriction.

Funding

This work was financially supported by the National Key Research and Development Program of China (2022YFB3807101/2022YFB3807102/2022YFB3807100), the National Science Fund for Distinguished Young Scholars (52025034) Key Research and Development Program of Shaanxi Province (2023-YBGY-193), Natural Science Foundation Project of Chongqing (CSTB2022NSCQ-MSX0565).

Credit authorship contribution statement

Yuzhang Du: Investigation, Conceptualization, Methodology, Validation, Formal analysis, Data Curation, Visualization, Writing-Original Draft, Funding Acquisition.

Wenxuan Lu, Yichen Liu, Rui Yu and Panzhen Wu: Methodology, Formal analysis, Data Curation, Visualization

Jie Kong: Investigation, Conceptualization, Resources, Funding Acquisition.

References

1. Su T, Liu N, Lei D, Wang L, Ren Z, Zhang Q, Su J, Zhang Z, Gao Y (2022) Flexible MXene/bacterial cellulose film sound detector based on piezoresistive sensing mechanism. ACS Nano 16:8461–8471
2. Colletti L, Murray EH (2023) Voice onset time in children with and without vocal fold nodules. J Speech Lang Hear Res 66:1467–1478
3. Chen M, Ma Y, Li Y, Wu D, Zhang Y, Youn C-H (2017) Wearable 20: Enabling human-cloud integration in next generation healthcare systems. IEEE Commun Mag 55:54–61
4. Chung PJ, Patel DR, Nizami I (2020) Disorder of written expression and dysgraphia: definition, diagnosis, and management. Trans Pediatr 9:S46–S54
5. Whitfield JA, Reif A, Goberman AM (2018) Voicing contrast of stop consonant production in the speech of individuals with parkinson disease on and off dopaminergic medication. Clin Linguist Phonet 32:587–594
6. Darweesh ME, Elsady SR, Reifaie NA, Sidhom RM (2020) Dysgraphia: Evaluating an arabic training program for remediation of egyptian dysgraphic children. Egypt J Otolaryngol 36:43
7. Devi A, Kavya G (2023) Dysgraphia disorder forecasting and classification technique using intelligent deep learning approaches. Prog Neuro-Psychoph 120:110647
8. Dinh Le TS, An J, Huang Y, Vo Q, Boonruangkan J, Tran T, Kim SW, Sun G, Kim YJ (2019) Ultrasensitive anti-interference voice recognition by bio-inspired skin-attachable self-cleaning acoustic sensors. ACS Nano 13:13293–13303
9. Su Y, Ma K, Zhang X, Liu M (2022) Neural network-enabled flexible pressure and temperature sensor with honeycomb-like architecture for voice recognition. Sensors 22:759

10. Blumrosen G, Sakuma K, Rice JJ, Knickerbocker J (2020) Back to finger-writing: fingertip writing technology based on pressure sensing. Ieee Access 8:35455–35468
11. Yang J, Chen J, Su Y, Jing Q, Li Z, Yi F, Wen X, Wang Z, Wang ZL (2015) Eardrum-inspired active sensors for self-powered cardiovascular system characterization and throat-attached anti-interference voice recognition. Adv Mater 27:1316–
12. Lan B, Yang T, Tian G, Ao Y, Jin L, Xiong D, Wang S, Zhang H, Deng L, Sun Y, Zhang J, Deng W, Yang W (2023) Multichannel gradient piezoelectric transducer assisted with deep learning for broadband acoustic sensing. ACS Appl Mater Interfaces DOI 101021/acsami2c20520
13. Zhang X, Wang Y, Zhao W, Wei W, Tao Z, Zhao H (2020) Vocal cord abnormal voice flow field study by modeling a bionic vocal system. Adv Rob 34:28–36
14. Husson R (1957) Vibration of the vocal cords in man without air passage and the role of an eventual sub-glottic pressure. J Physiologie 49:217–220
15. Hochhauser M, Wagner M, Shvalb N (2023) Assessment of children's writing features: a pilot method study of pen-grip kinetics and writing surface pressure. Assist Technol 35:107–115
16. Steinwachs KC, Fehm HL (1988) Effects of the neuropeptide plg(l-prolyl-leucyl-glycinamide) on writing pressure and speed in healthy-subjects. Pharmacopsychiatry 21:459–460
17. Garcia JR, McCrystal M, Horvath D, Kaur H, Carey T, Coleman JN (2023) Tuneable piezoresistance of graphene-based 2d:2d nanocomposite networks. Adv Funct Mater 33:2307956
18. Wang Y, Yue Y, Cheng F, Cheng Y, Ge B, Liu N, Gao Y (2022) $Ti_3C_2T_x$ mxene-based flexible piezoresistive physical sensors. ACS Nano 16:1734–1758
19. Zhao XH, Ma SN, Long H, Yuan H, Tang CY, Cheng PK, Tsang YH (2018) Multifunctional sensor based on porous carbon derived from metal-organic frameworks for real time health monitoring. ACS Appl Mater Interfaces 10:3986–3993
20. Yang Y, Shi L, Cao Z, Wang R, Sun J (2019) Strain sensors with a high sensitivity and a wide sensing range based on a $TI_3C_2T_X$ (MXene) nanoparticle-nanosheet hybrid network. Adv Funct Mater 29:1807882
21. Chen W, Liu L-X, Zhang H-B, Yu Z-Z (2021) Kirigami-inspired highly stretchable conductive and hierarchical $TI_3C_2T_X$ mxene films for efficient electromagnetic interference shielding and pressure sensing. ACS Nano 15:7668–7681
22. Du Y, Yu G, Dai X, Wang X, Yao B, Kong J (2020) Highly stretchable self-healable ultrasensitive strain and proximity sensors based on skin-inspired conductive film for human motion monitoring. ACS Appl Mater Interfaces 12:51987–51998
23. Shi X, Wang H, Xie X, Xue Q, Zhang J, Kang S, Wang C, Liang J, Chen Y (2019) Bioinspired ultrasensitive and stretchable mxene-based strain sensor via nacre-mimetic microscale brick-and-mortar architecture. ACS Nano 13:649–659
24. Ma C, Ma M-G, Si C, Ji X-X, Wan P (2021) Flexible mxene-based composites for wearable devices. Adv Funct Mater 31:2009524

25. Du Y, Wang X, Dai X, Lu W, Tang Y, Kong J (2022) Ultraflexible highly efficient electromagnetic interference shielding and self-healable triboelectric nanogenerator based on $Tl_3C_2T_X$ mxene for self-powered wearable electronics. J Mater Sci Technol 100:1–11
26. Yin Z, Hannard F, Barthelat F (2019) Impact-resistant nacre-like transparent materials. Science 364:1260–
27. Xu Z-H, Li X (2011) Deformation strengthening of biopolymer in nacre. Adv Funct Mater 21:3883–3888
28. Luo C-L, Jiao J-Y, Su X-J, Zheng L-X, Yan W-G, Zhong D-Z (2022) Interlinked microcone resistive sensors based on self-assembly carbon nanotubes film for monitoring of signals. Nanomaterials 12:2325
29. Qu C, Lu M, Zhang Z, Chen S, Liu D, Zhang D, Wang J, Sheng B (2023) Flexible microstructured capacitive pressure sensors using laser engraving and graphitization from natural wood. Molecules 28:5339
30. Chen W, Yan X (2020) Progress in achieving high-performance piezoresistive and capacitive flexible pressure sensors: A review. J Mater Sci Technol 43:175–188
31. Wegst UGK, Bai H, Saiz E, Tomsia AP, Ritchie RO (2015) Bioinspired structural materials. Nat Mater 14:23–36
32. Meyers MA, McKittrick J, Chen P-Y (2013) Structural biological materials: critical mechanics-materials connections. Science 339:773–779
33. Su E, Wu F, Zhao S, Li Y, Deng C (2022) Layered MXene/aramid composite film for a soft and sensitive pressure sensor. ACS Appl Mater Interfaces 14:15849–15858
34. Texido R, Nieva-Esteve G, Gilabert-Porres J, Reyes G, Borros S (2023) Highly sensitive silver-microlayer thin film on a pp-pfm-modified pdms strain sensor as a versatile tool for stretchable electronics applications. Adv Electron Mater DOI 101002aelm202200717
35. Li X-P, Li Y, Li X, Song D, Min P, Hu C, Zhang H-B, Koratkar N, Yu Z-Z (2019) Highly sensitive reliable and flexible piezoresistive pressure sensors featuring polyurethane sponge coated with MXene sheets. J Colloid Interf Sci 542:54–62
36. Guo Y, Zhong M, Fang Z, Wan P, Yu GA (2019) Wearable transient pressure sensor made with MXene nanosheets for sensitive broad-range human-machine interfacing. Nano Lett 19:1143–1150
37. Liu R, Li J, Li M, Zhang Q, Shi G, Li Y, Hou C, Wang H (2020) MXene-coated air-permeable pressure-sensing fabric for smart wear. ACS Appl Mater Interfaces 12:46446–46454
38. Zhao J, Gao J, Zhou Z, Gui J, Wang Y, Wu X, Li M, Xu R (2021) Highly responsive asymmetric pressure sensor based on MXene/reduced graphene oxide nanocomposite fabricated by laser scribing technique. Ieee Sens J 21:26673–26680
39. Yang Z, Lv S, Zhang Y, Wang J, Jiang L, Jia X, Wang C, Yan X, Sun P, Duan Y, Liu F, Lu G (2022) Self-assembly 3D porous crumpled MXene spheres as efficient gas and pressure sensing material for transient all-MXene sensors. Nano-Micro Lett 14:56

40. Yu Q, Su C, Bi S, Huang Y, Li J, Shao H, Jiang J, Chen N (2022) $Ti_3C_2T_X$@nonwoven fabric composite: promising mxene-coated fabric for wearable piezoresistive pressure sensors. ACS Appl Mater Interfaces 14:9632–9643
41. Li T, Chen L, Yang X, Chen X, Zhang Z, Zhao T, Li X, Zhang JA (2019) Flexible pressure sensor based on an mxene-textile network structure. J Mater Chem C 7:1022–1027
42. Zheng Y, Yin R, Zhao Y, Liu H, Zhang D, Shi X, Zhang B, Liu C, Shen C Conductive MXene/cotton fabric based pressure sensor with both high sensitivity and wide sensing range for human motion detection and e-skin. Chem Eng J 420: 127720
43. An J, Ma Y, He M, Yan J, Zhang C, Li X, Shen P, Luo S, Gao Y (2020) A wearable and highly sensitive textile-based pressure sensor with $TI_3C_2T_X$ nanosheets sensors. Actuat a-Phys 311:122081
44. Ma Y, Cheng Y, Wang J, Fu S, Zhou M, Yang Y, Li B, Zhang X, Nan C-W (2022) Flexible and highly-sensitive pressure sensor based on controllably oxidized MXene. Infomat 4:e12328
45. Lou Z, Chen S, Wang L, Shi R, Li L, Jiang K, Chen D, Shen G (2017) Ultrasensitive and ultraflexible e-skins with dual functionalities for wearable electronics. Nano Energy 38:28–35
46. Wan S, Zhang Q, Zhou X, Li D, Ji B, Jiang L, Cheng Q (2017) Fatigue resistant bioinspired composite from synergistic two-dimensional nanocomponents. ACS Nano 11:7074–7083
47. Berezovsky J (2019) The structure of musical harmony as an ordered phase of sound: a statistical mechanics approach to music theory. Sci Adv 5:eaav8490
48. Wang Y, Yang T, Lao J, Zhang R, Zhang Y, Zhu M, Li X, Zang X, Wang K, Yu W, Jin H, Wang L, Zhu H (2015) Ultra-sensitive graphene strain sensor for sound signal acquisition and recognition. Nano Res 8:1627–1636
49. Choi H-M, Ju-Hwan L (2021) The effect of sound level of reactive dialogue on emotional evaluation of video content. J Digit Content Soc 22:1997–2004
50. Liu Z, Li X, Du S, Chen W, Shao J, Zheng Q (2021) Strategy and implementing techniques for the sound quality target of car interior noise during acceleration. Appl Acoust 182:108171
51. Tseng MH, Chow SM (2000) Perceptual-motor function of school-age children with slow handwriting speed. Am J Occup Ther 54:83–88

Figures

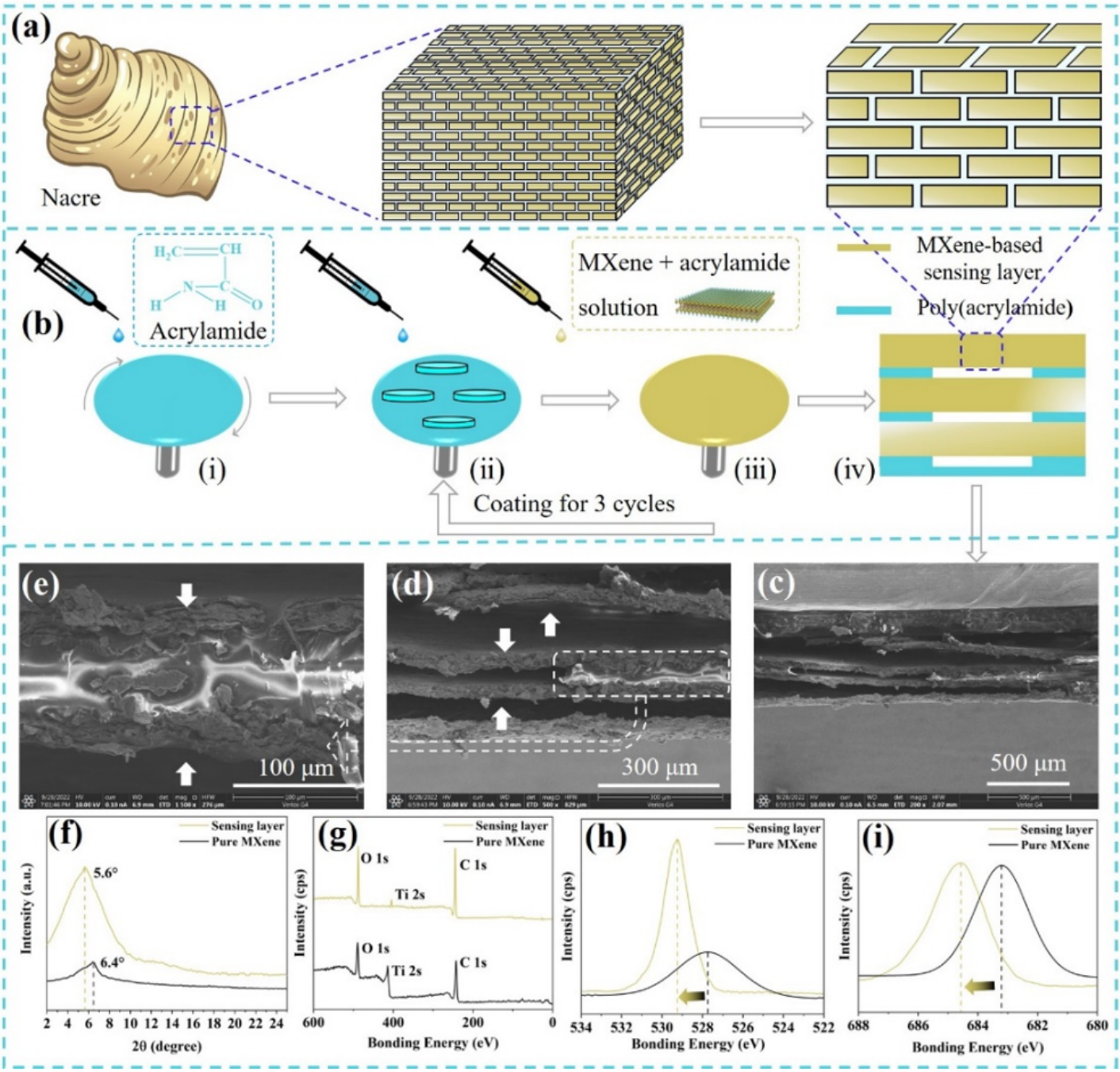

Figure 1

The fabrication of pressure sensor with the enhanced interfacial interactions in sensing layers and air gaps in device. (a) Schematic drawing of the hierarchical structure of nature nacre with strong interfacial interactions that resulted from the bonding between aragonite platelets (95 vol%) and nanofibrillar chitin and proteins (5 vol%). (b) Schematic illustration of the fabrication procedure for pressure sensor via LBL assembly. ( ) Spin coating acrylamide aqueous solution ( ) dropwise adding acrylamide aqueous solution at different sites on the surface of PAM flexible substrate ( ) the fabrication of MXene-based sensing layer by coating the mixed solution of MXene and acrylamide ( ) steps and were repeated for three cycles to prepare pressure sensor. (c-e) The SEM images show that the resultant sensor with well-defined multilayer

structure and air gaps in device (c d) and the adjacent sensing layers tightly jointed by PAM polymer (e). (f) XRD patterns of pure MXene and MXene-based sensing layer. (g-i) XPS spectra (g) and high resolution XPS spectra for O (h) and F element (i) of sensing layer and pure MXene.

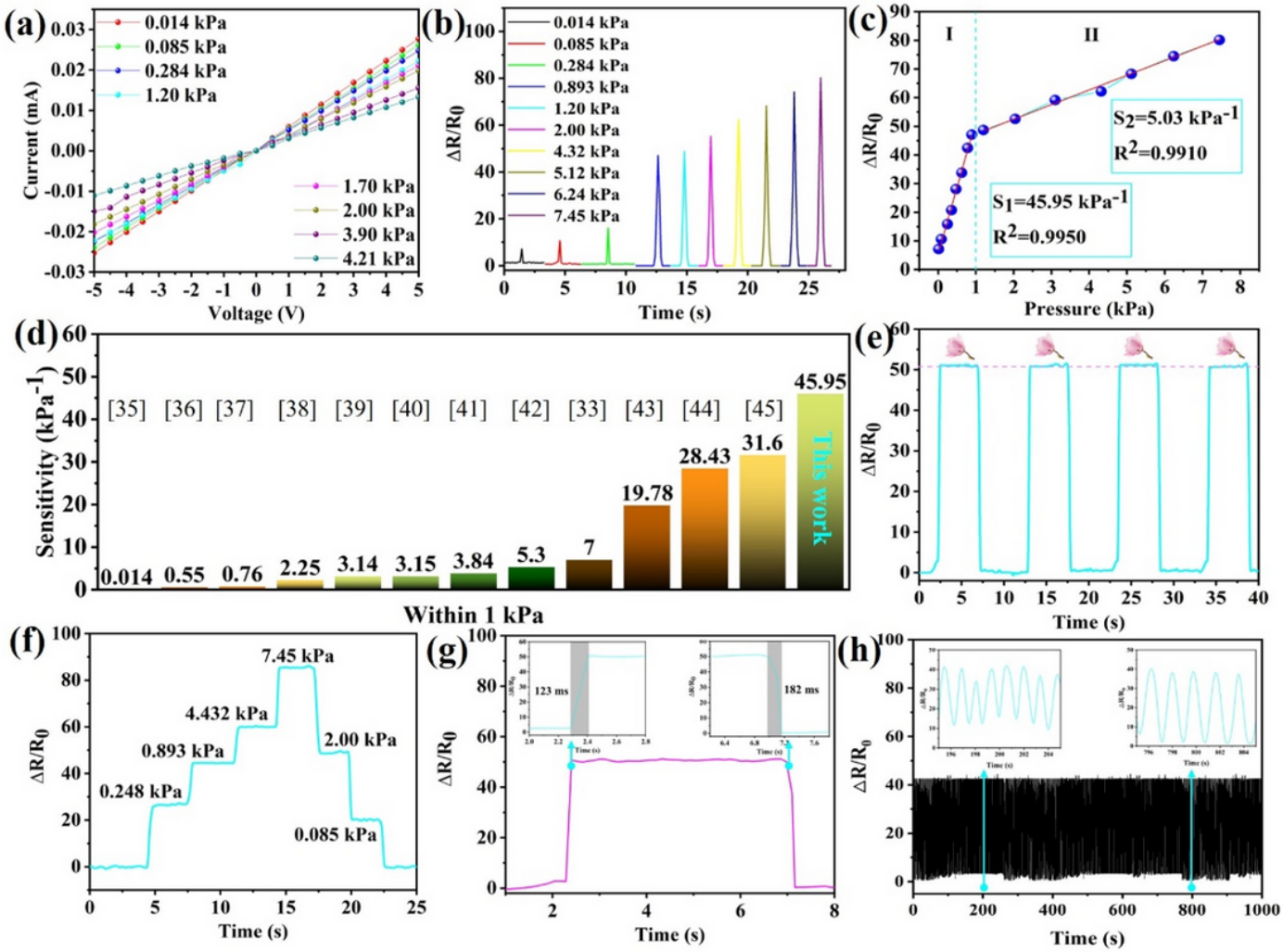

Figure 2

Ultrahigh sensitivity and sensing performance of the resultant pressure sensor. (a) The *I*– *V* curves of sensor under serial pressures. (b) Electrical signals produced by loading various pressures on sensor. (c) Relative resistance change ($\Delta R/R_0$) as a function of the applied pressure in the range of 0–7.45 kPa. Sensitivity (S) and linear behavior of sensor in pressure range of 0–1 kPa (S=45.95 kPa^{-1} R^2=0.9950) and 1–7.45 kPa (S=5.03 kPa^{-1} R^2=0.9910) respectively. (d) The comparison of sensitivity within pressure less than 1 kPa between this work and the previously reported pressure sensors [33, 35-45]. (e) $\Delta R/R_0$ values of sensor under periodic loading–unloading cycles with a constant pressure of 0.893 kPa. (f) Electrical signals obtained by loading various pressures on sensor for about 3s. (g) The response and recovery time of the sensor. (i) The durability measurement under cyclic loading–unloading at 0.893 kPa for 2 000 cycles.

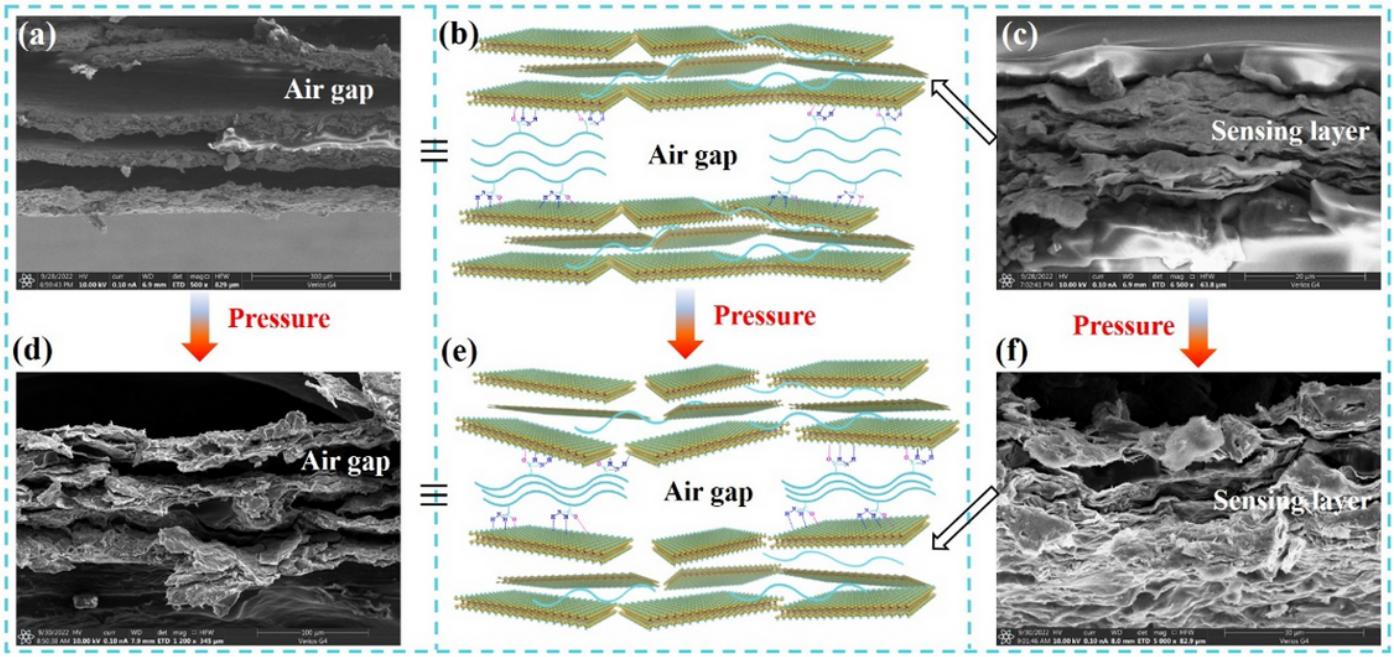

Figure 3

Sensing mechanism based on crack-propagation facilitated by the synergistic effects of air gaps and hydrogen bond interfacial interactions. (a-b) Cross-sectional SEM image (a) and schematic drawing (b) showing the initial architecture of the as-prepared pressure sensor and the air gaps constructed in device. (d-e) SEM image (d) and schematic illustration (e) of structure of sensor after suffering pressure. (c f) Cross-sectional SEM image of sensing layer before (c) and after loading pressure of 0.893 kPa (f).

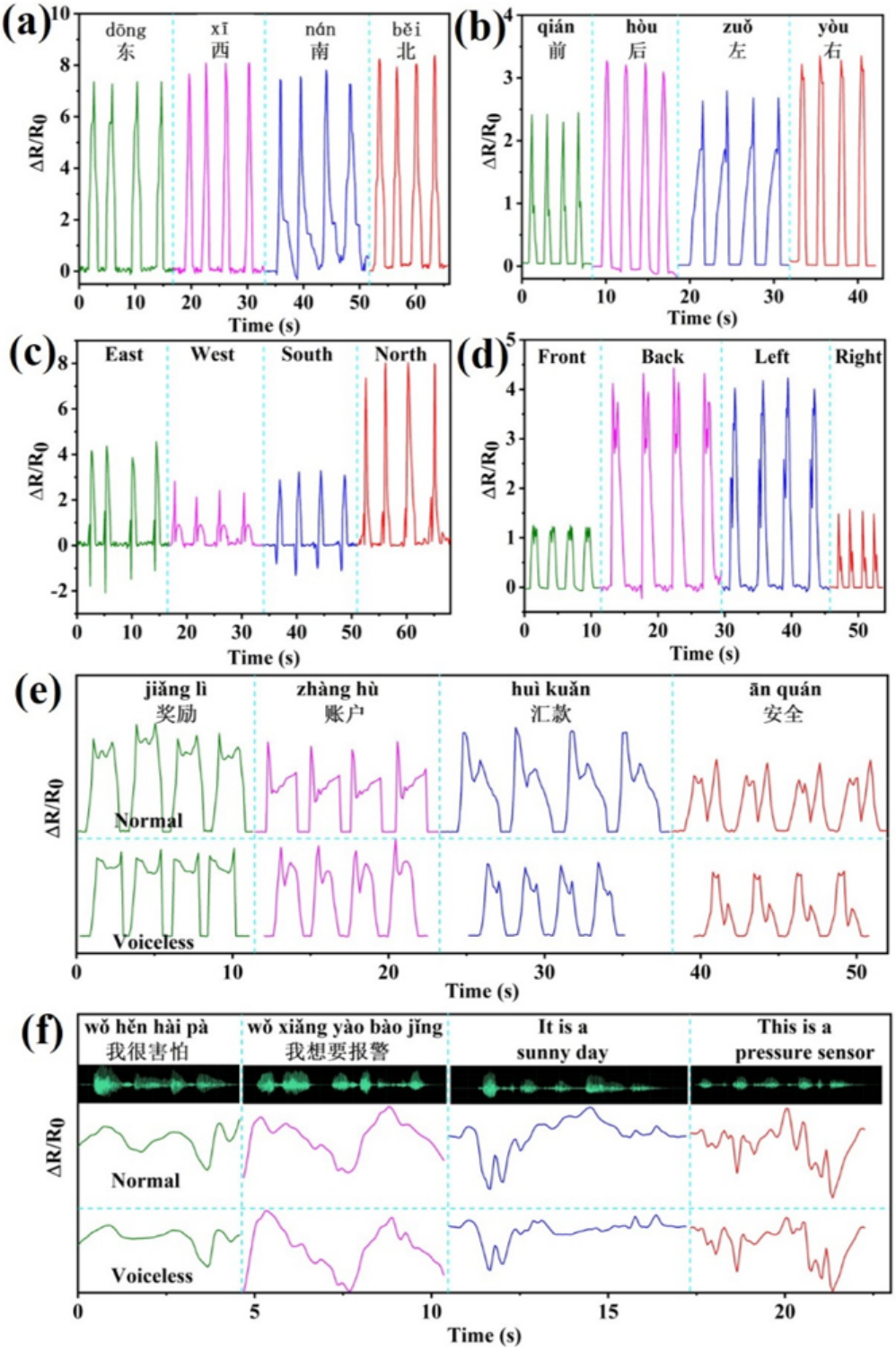

Figure 4

The recognition of normal and “voiceless” speaking. (a-d) Electrical signals with single peak (a-b) and multiple peaks (c-d) induced by normally speaking Chinese words and English words respectively. (e-f) The curves induced by the simulated “voiceless” speaking and normal speaking showing a good coincidence.

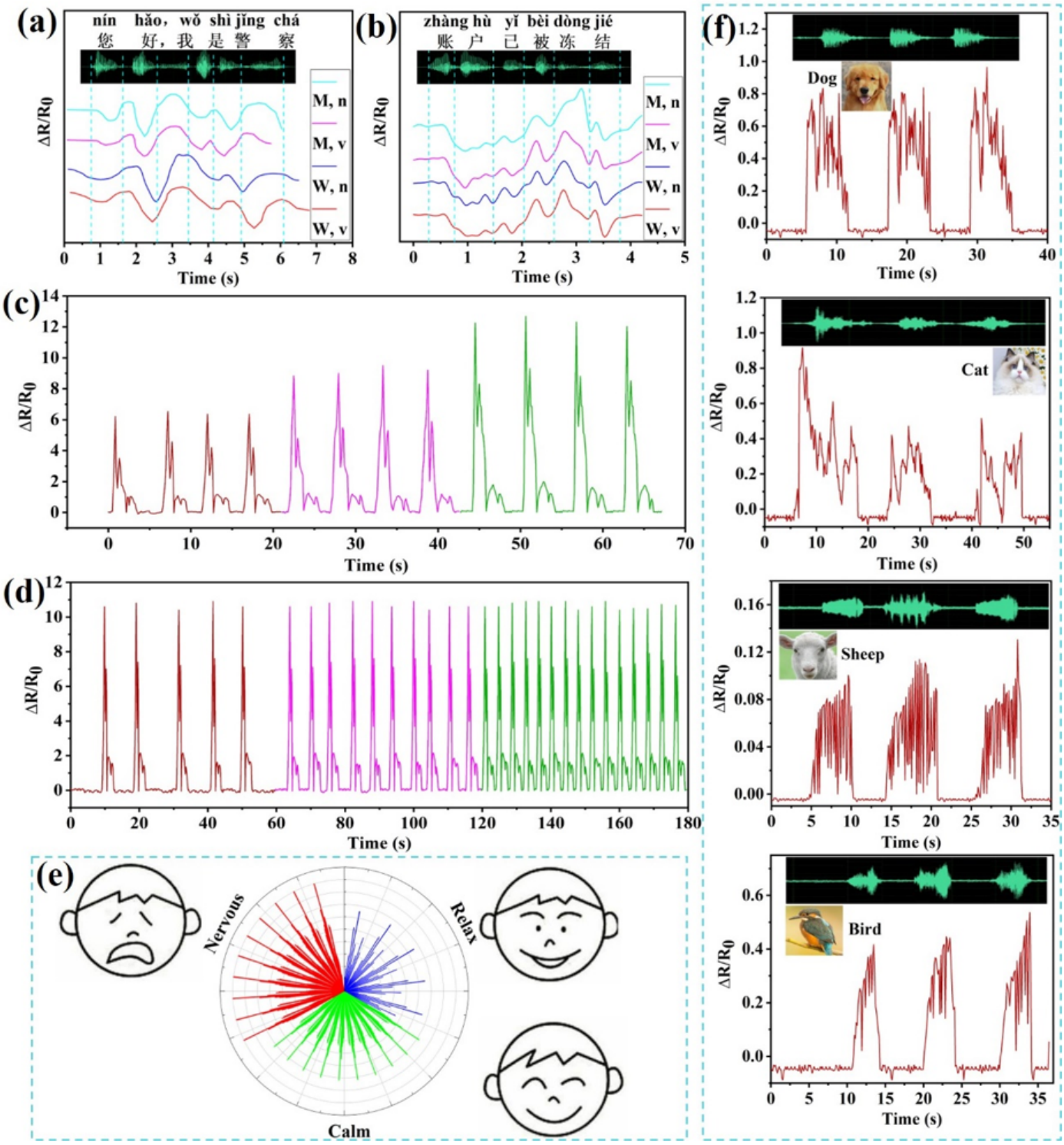

Figure 5

High recognition performance of sound volume frequency and environment noise. (a b) The comparison of signals resulted from man and woman speaking different Chinese sentences in voiceless or normal manner. “M n” and “W n” represents man or woman speaking normal while “M v” and “W v” is man or women voiceless speaking. (c d) The response to the voiceless speaking with various volume (c) and

frequencies (d). (e) Wind-rose map visually displaying the relaxed calm and nervous motion. (f) Superior detecting performance of animal acoustic activities.

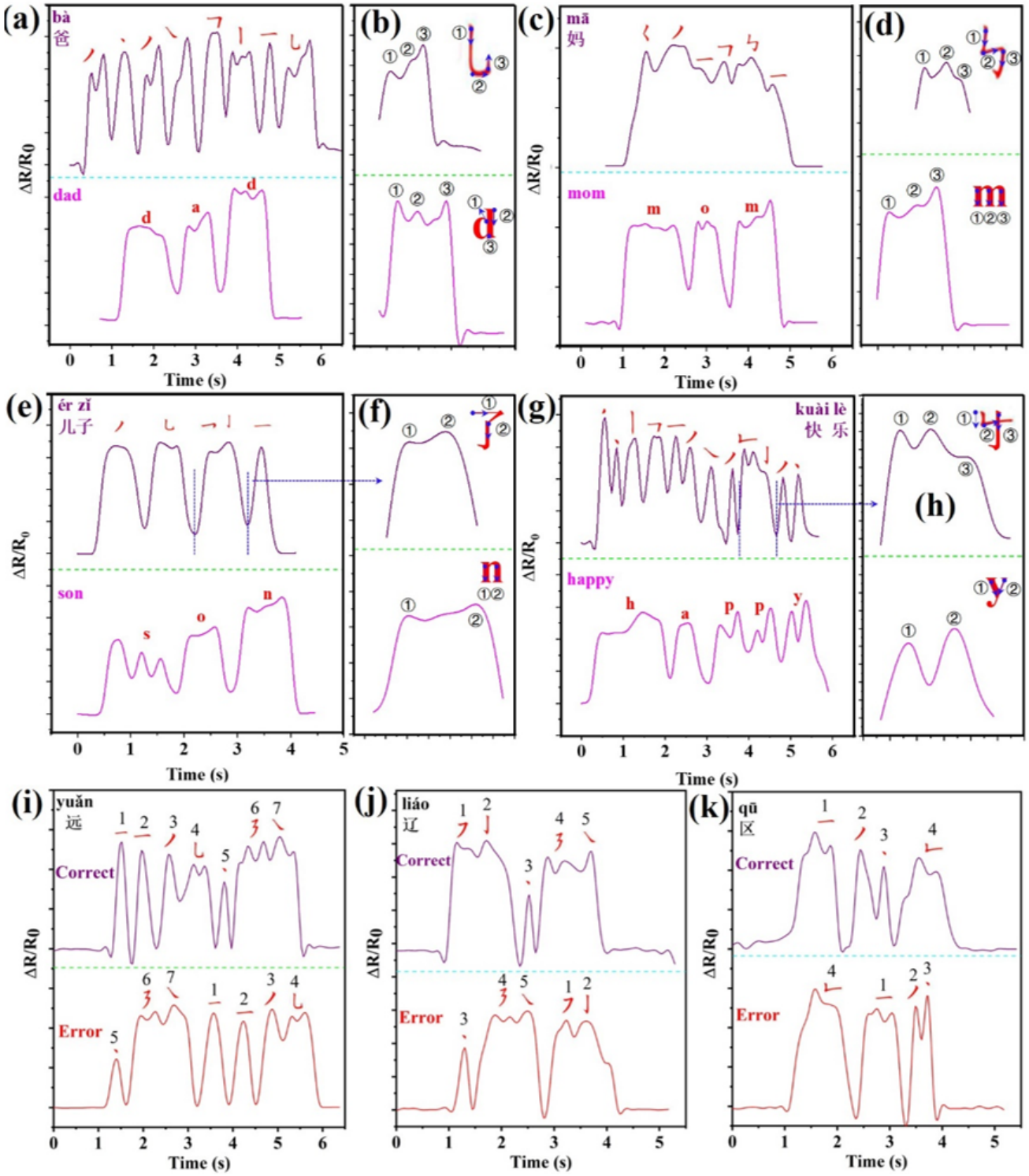

Figure 6

High sensing sensitivity to stroke order of Chinese characters and English words. (a) Different Characteristic peaks caused by the different strokes of Chinese character “ ” and English word “dad”. (b)

There are three characteristic peaks induced by and three power points of Chinese character stroke “ ” (up) or English letter “d” (down) respectively. (c e g) The single curves obtained from recognizing the different Chinese characters (up) as well as the corresponding English words (down). (d f h) The enlarged images show that the multiple characteristic peaks induced by the different power points of Chinese character stroke or English letter. (i-k) The comparison of signal curves between writing with correct (up) and error (down) stroke order.

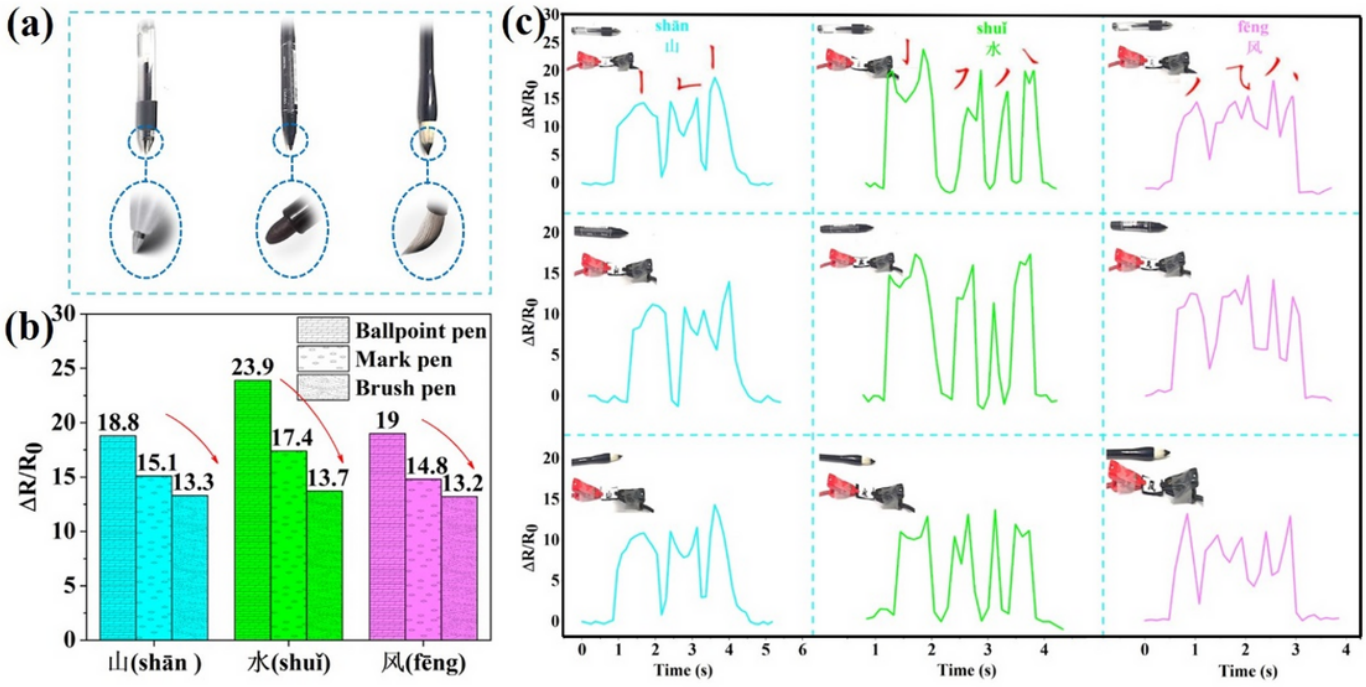

Figure 7

The recognition of writing with poor hand strength. (a) Three different kinds of pen with various tip hardness (ballpoint pen mark pen brush pen) were employed to simulate the different hand strength. (b) Column diagram exhibits the using of the pen with lower hardness to write character leading a little $\Delta R/R_0$ value. (c) The comparison of signal curves obtained from recognizing writing by using different pen.

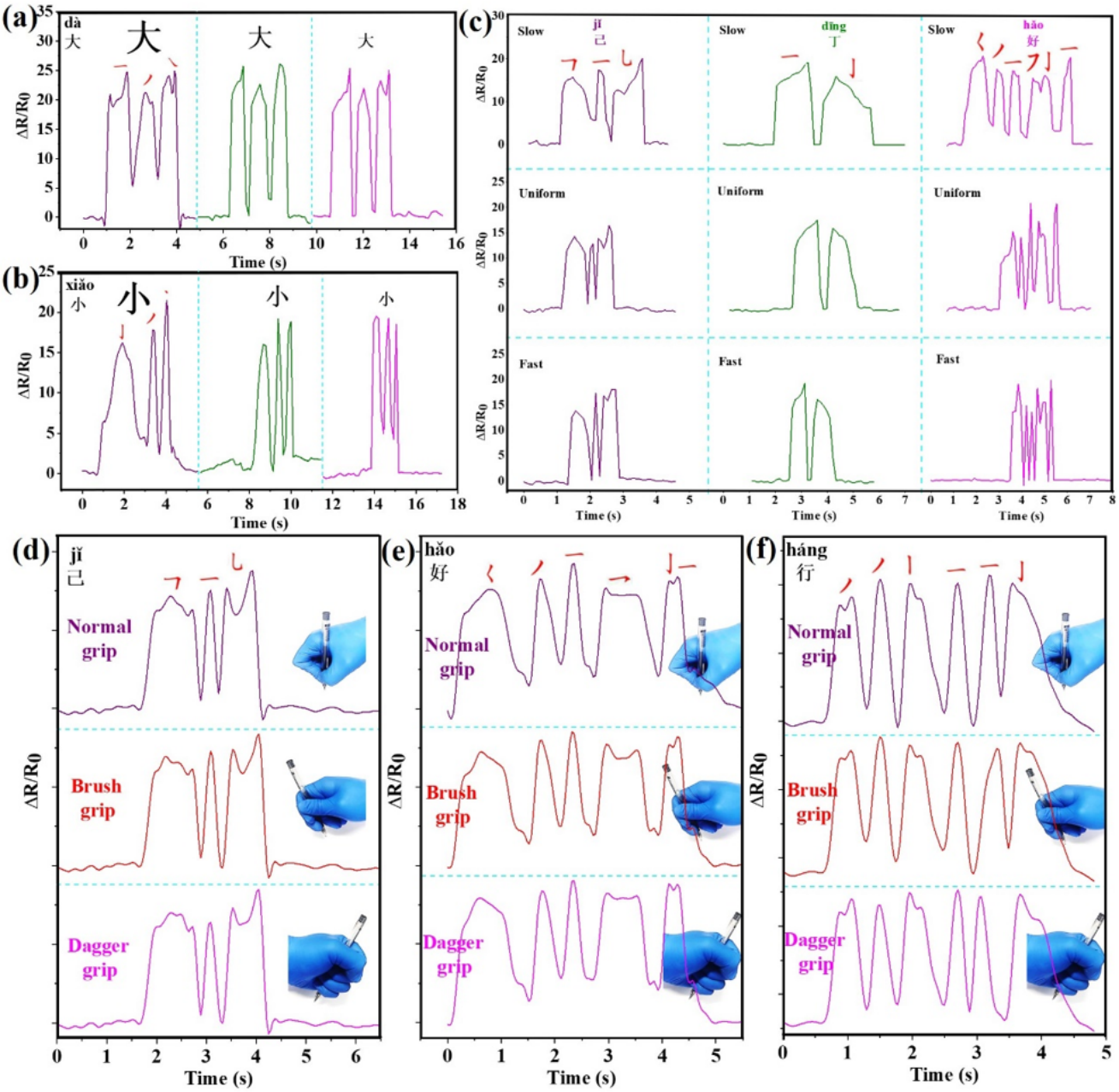

Figure 8

The good recognition performance of writing with different character size writing speed as well as grip of the pen.(a-c) Electrical signals acquired from monitoring writing with different character size (a b) and various writing speed (c). (d-f) Signal curves recorded by writing different Chinese characters performed under correct or error grip of the pen. The writing content from special groups with dysgraphia can be well read by comparing with the signal curve obtained in the normal writing manner.

Supplementary Files

This is a list of supplementary files associated with this preprint. Click to download.

- SupportingInformation.docx